



Real space density-constrained time-dependent Hartree-Fock-Bogoliubov method and pairing effects in the fusion of calcium isotopes

Liang Tong  and Shiwei Yan ^{*}*Department of Physics, Beijing Normal University, Beijing 100875, China*

(Received 16 August 2021; accepted 10 January 2022; published 18 January 2022)

To describe the fusion cross sections with a method that includes the superfluidity and to understand the impact of pairing on both the fusion barrier and cross sections, we propose a real-space particle- and pairing-density-constrained scheme of the time-dependent Hartree-Fock-Bogoliubov (TDHFB) method and a definition of TDHFB particle current. Using the GOGNY-TDHFB code, this scheme is applied to investigate the fusion reactions of $^{40}\text{Ca} + ^{40}\text{Ca}$, $^{40}\text{Ca} + ^{44}\text{Ca}$, and $^{40}\text{Ca} + ^{48}\text{Ca}$ by comparison. The results show that this density-constrained TDHFB scheme is reliable for analysis of the collision processes involved with superfluid nuclei.

DOI: [10.1103/PhysRevC.105.014613](https://doi.org/10.1103/PhysRevC.105.014613)

I. INTRODUCTION

Heavy-ion fusion reactions provide important information about the essential structure and dynamic evolution of nuclear many-body systems. Microscopic quantum theories are indispensable for understanding fusion reactions at near-barrier energies because the dynamics of the fusion process and the influence of shell and pairing effects are considered to be essential assets.

Since the decisive paper by Hill and Wheeler [1], the large-amplitude collective motions of a nucleus are mainly discussed within the adiabatic approximation, where the nucleons follow the time-dependent (self-consistent) potential along the single-particle eigenstates. As functions of the collective variable, the single-particle energies vary and quasicrossing of the energy levels occurs when the repulsion of a pair of energy levels takes place. Close to such quasicrossing of adjacent levels, the adiabatic wave functions change rapidly, which introduces large dynamical coupling among the wave functions in the time-dependent treatment of nuclear collective motion. The dynamical couplings give rise to large difficulties both conceptually and numerically, in particular at finite excitation energies.

When two colliding nuclei approach each other and the shape of system undergoes sudden changes, the adiabatic approximation is expected to break down and the evolution occurs along diabatic single-particle levels rather than along adiabatic single-particle levels, which can be attributed to the residual interactions [2]. The friction coefficient of dissipative dynamics can be extracted by the time-dependent microscopic mean field theory [3]. A study with the quantum molecular dynamics model [4] has shown that the mean field may play a dominant role in energy dissipation in the approach stage of the two colliding nuclei. After the system passes the Coulomb

barrier, the pure mean-field theory gives an unphysical behavior of the friction coefficient [4], which gives evidence that two-body collisions are important in fusion reactions.

Pairing correlations are believed to play a crucial role in causing the two-body dissipation and/or the Landau-Zener effect [5–8]. From a dynamical point of view, time-dependent density functional theory is an ideal tool to study the fusion dynamics as it is a fully microscopic and nonadiabatic approach. In order to consider pairing correlations, a theoretical scheme combining the time-dependent Hartree-Fock (TDHF) theory with BCS approximation (TDHF-BCS) [5,9] has been proposed to study the fusion dynamics of neutron-rich light nuclei in the near-barrier domain [10]. It is very successful in reproducing the fusion cross section without any adjusted parameter. However, the TDHF-BCS approach does not respect the continuity equation, which may lead to nonphysical results in specific cases such as particle emission [11]. In order to avoid this drawback, the frozen occupation approximation has to be adopted, i.e., the occupation numbers are frozen at their initial values and do not change as the reaction dynamics proceed [10,11].

For more realistic treatment of the impact of pairing on the fusion dynamics, it is desirable to carry out microscopic calculations in which the pairing effects are allowed to vary in response to the shape changes of the nuclear system as the fusion proceeds. A reasonable candidate of the theoretical framework is the time-dependent Hartree-Fock-Bogoliubov (TDHFB) theory which self-consistently includes dynamic pairing correlations [12–14]. In TDHFB calculations, the pairing correlations account partly for the Landau-Zener effect, so the two-body dissipation is partially considered [5–8].

A density-constrained method of TDHFB theory was proposed in [15] following the density-constrained TDHF method (DC-TDHF) developed in [16,17]. In those methods, the interaction potential between the colliding nuclei as well as a coordinate dependent mass are extracted from the density-constrained calculations. The resultant potentials and masses

^{*}Corresponding author: yansw@bnu.edu.cn

can then be applied to calculate the fusion cross section in a one-dimensional barrier penetration model. In this sense, such methods combined with the one-dimensional barrier penetration model can describe the barrier penetration of the full many-body system.

In realistic implementation of the density-constrained calculation proposed in [15], the iteration process is rather unstable and difficult to get convergent solutions of constrained-HFB equations (Eq. (13) in [15]) when the constraints on pairing tensor are taken into account. The reason might be that all the matrix elements of pairing tensor are considered in configuration space. The constraint terms related to the pairing tensors change frequently, specially after the fusing system passes the barrier top region.

Based on this consideration, in this paper we introduce the constraints on both density matrix and pairing tensor in real space, abbreviated rDC-TDHFB in the following, so that the one-body particle and pairing densities are treated in a parallel way, as shown in Sec. II. With this real-space density-constrained scheme of the rDC-TDHFB method, we analyzed the low energy head-on collision reactions of $^{40}\text{Ca} + ^{40}\text{Ca}$, $^{40}\text{Ca} + ^{44}\text{Ca}$, and $^{40}\text{Ca} + ^{48}\text{Ca}$ systems and we show impact of pairing dynamics on fusion in Sec. III. Finally, a short summary is given in Sec. IV.

II. RDC-TDHFB METHOD IN REAL SPACE

We use the GOGNY-TDHFB code [14,15] to simulate the dynamic evolutions of the fusion process and follow the main procedures proposed in [15–17] to implement the density constraints on the TDHFB trajectories. The density-constrained many-body states of a system are obtained through minimizing

$$\delta \left\langle \Phi \left| H - \sum_{\mathbf{r}} \lambda(\mathbf{r}) [\rho(\mathbf{r}) - \rho^{(0)}(\mathbf{r}, t)] - \sum_{\mathbf{r}} \lambda_{\uparrow\downarrow}^{(2)}(\mathbf{r}) [\kappa_{\uparrow\downarrow}(\mathbf{r}) - \kappa_{\uparrow\downarrow}^{(0)}(\mathbf{r}, t)] \right| \Phi \right\rangle = 0, \quad (1)$$

with H the HFB Hamiltonian of the system, $\sigma = \uparrow, \downarrow$ the z projection of the nucleon spin, $\rho^{(0)}(\mathbf{r}, t)$ and $\kappa_{\uparrow\downarrow}^{(0)}(\mathbf{r}, t)$ the instantaneous TDHFB particle and pairing densities in real space, and $\lambda(\mathbf{r})$ and $\lambda_{\uparrow\downarrow}^{(2)}(\mathbf{r})$ the Lagrange multipliers of the one-body particle and pairing densities, respectively. Consequently, the system goes down to the minimum-energy state

described by the HFB state $|\Phi\rangle$ by keeping all the TDHFB dynamical features, such as the one-body particle and pairing density distributions, collective deformation, etc.

The hybrid bases $\phi_{\alpha}(\mathbf{r})$ are used for calculating the one-body particle and pairing densities, $\rho(\mathbf{r})$ and $\kappa_{\sigma\sigma'}(\mathbf{r})$, in which two-dimensional harmonic oscillator eigenfunctions are used in the xy plane while a Lagrange mesh [18] is used in the z direction [14]. The notation α is for a set of numbers $\alpha = \{n_x, n_y, z, \sigma\}$. The local particle and pairing densities in real space at certain times t are obtained as follows:

$$\rho(\mathbf{r}) = \sum_{\alpha\beta} \phi_{\beta}^*(\mathbf{r}) \phi_{\alpha}(\mathbf{r}) \rho_{\alpha\beta} \delta_{\sigma_{\alpha}\sigma_{\beta}}, \quad (2a)$$

$$\kappa_{\uparrow\downarrow}(\mathbf{r}) = \sum_{\alpha\beta} \phi_{\beta}(\mathbf{r}, \downarrow) \phi_{\alpha}(\mathbf{r}, \uparrow) \kappa_{\alpha\beta}, \quad (2b)$$

and $\kappa_{\downarrow\uparrow}(\mathbf{r}) = -\kappa_{\uparrow\downarrow}(\mathbf{r})$ due to $\kappa_{\beta\alpha} = -\kappa_{\alpha\beta}$ [19].

To minimize HFB energy with Eq. (1), the Lagrange multipliers, $\lambda(\mathbf{r})$ and $\lambda_{\uparrow\downarrow}(\mathbf{r})$, are updated by

$$\lambda^{(n+1)}(\mathbf{r}) = \lambda^{(n)}(\mathbf{r}) + \frac{a_1}{\rho(\mathbf{r}) + d_1} [\rho(\mathbf{r}) - \rho^{(0)}(\mathbf{r})], \quad (3a)$$

$$\lambda_{\uparrow\downarrow}^{(2)(n+1)}(\mathbf{r}) = \lambda_{\uparrow\downarrow}^{(2)(n)}(\mathbf{r}) + \Delta \lambda_{\uparrow\downarrow}^{(2)}(\mathbf{r}), \quad (3b)$$

where

$$\Delta \lambda_{\uparrow\downarrow}^{(2)}(\mathbf{r}) = a_2 \frac{\kappa_{\uparrow\downarrow}(\mathbf{r})}{|\kappa_{\uparrow\downarrow}(\mathbf{r})|} [|\kappa_{\uparrow\downarrow}(\mathbf{r})| - |\kappa_{\uparrow\downarrow}^{(0)}(\mathbf{r})|] \sqrt{|\kappa_{\uparrow\downarrow}^{(0)}(\mathbf{r})|}. \quad (4)$$

After examining the iteration processes, we suggest the parameters a_1 , a_2 , and d_1 in the regions $-30 \leq a_1 \leq -5$ MeV, $10|a_1| < a_2 < 30|a_1|$, and $d_1 = 0.5\text{fm}^{-3}$, respectively.

Here we would like to mention that, after nuclei pass over the barrier top in the fusion process, pairing excitations will become massive and cause single-particle level-crossings and thus induce Landau-Zener transitions [7,8]. In this case, to set up the constraint on the particle densities with the conserved total number of particles only might not be enough to ensure complete squeeze-out of the collective kinetic and excitation energies from the total energy of TDHFB trajectory. The constraint on the pairing densities might be indispensable to obtain a reasonable dynamical potential when the two colliding nuclei are largely overlapped. We will explain this point further in the following.

Under the definitions of the constrained scheme in Eqs. (3) and (4), the constrained HFB equation (1) can be explicitly expressed as

$$\begin{pmatrix} h_{\uparrow\uparrow} - \lambda - \lambda_{\uparrow\uparrow}^{HF} & h_{\uparrow\downarrow} & 0 & \Delta - \lambda_{\uparrow\downarrow}^{(2)} \\ h_{\downarrow\uparrow} & h_{\downarrow\downarrow} - \lambda - \lambda_{\downarrow\downarrow}^{HF} & -\Delta + \lambda_{\downarrow\downarrow}^{(2)} & 0 \\ 0 & -\Delta^* + \lambda_{\uparrow\downarrow}^{(2)*} & -h_{\uparrow\uparrow}^* + \lambda + \lambda_{\uparrow\uparrow}^{HF} & -h_{\uparrow\downarrow}^* \\ \Delta^* - \lambda_{\uparrow\downarrow}^{(2)*} & 0 & -h_{\downarrow\uparrow}^* & -h_{\downarrow\downarrow}^* + \lambda + \lambda_{\downarrow\downarrow}^{HF} \end{pmatrix} \begin{pmatrix} U_{k\uparrow} \\ U_{k\downarrow} \\ V_{k\uparrow} \\ V_{k\downarrow} \end{pmatrix} = \epsilon_k \begin{pmatrix} U_{k\uparrow} \\ U_{k\downarrow} \\ V_{k\uparrow} \\ V_{k\downarrow} \end{pmatrix}. \quad (5)$$

where k labels the quasiparticle states. The single-particle Hamiltonian $h_{\sigma\sigma'}$ and the pairing field Δ are functionals of U and V matrices, ϵ_k is the energy spectrum of a quasiparticle, and λ is the chemical potential adjusted to conserve the total number of neutrons and protons. The constraint parameters

$\lambda_{\beta\alpha}^{HF}$ and $\lambda_{\beta\alpha}^{(2)}$ satisfy

$$\lambda_{\beta\alpha}^{HF} = \frac{\delta E_{\text{DC}}}{\delta \rho_{\alpha\beta}}, \quad \lambda_{\beta\alpha}^{(2)} = \frac{\delta E_{\text{DC}}}{\delta \kappa_{\alpha\beta}}, \quad (6)$$

where

$$E_{\text{DC}} = \frac{\langle \Phi | H | \Phi \rangle}{\langle \Phi | \Phi \rangle}, \quad (7)$$

with the density-constrained many-body wave function $|\Phi\rangle$ obtained through Eq. (1). Note that in the realistic implementation of the iteration, the instantaneous TDHFB wave functions are used as the initial iteration wave functions and the iteration process is accelerated using the modified Broyden method [20,21].

III. RESULTS AND DISCUSSIONS

In the studies of fusion dynamics, the pairing correlation is mainly considered in the ground states of projectile and target, because it is well known that the static pairing force is crucial for the description of the atomic nuclei, both in the ground state as well as in excited states. This viewpoint has been realized by the TDHF theory plus BCS model [10], where the frozen occupation approximation has been adopted, i.e., it is assumed that the main effects of the pairing correlations come from the initial correlations and the occupation numbers are frozen to their initial values as the reaction process goes on.

However, a recent study has shown that significant changes occur in the fusion dynamics when the dynamical effects of the pairing correlations are taken into account during the nuclear reactions in the time-dependent density functional theory [22]. The dynamic pairing correlations may affect inelastic excitations and multinucleon transfer probabilities [23].

In this paper, we studied the fusion reactions of three spherical Ca-based nuclei, $^{40}\text{Ca} + ^{40,44,48}\text{Ca}$, using the TDHFB theory based on GOGNY D1S parametrization. The experimental study of near- and sub-barrier fusion of calcium isotopes has a long background [24–28]. Meanwhile, the theoretical study has been implemented with the coupled-channels technique [29–33] and the microscopic TDHF theory coupled with a density-constrained approach [34]. Note that both the experimental and theoretical studies are mainly devoted to the investigations of reactions between normal nuclei, such as $^{40}\text{Ca} + ^{40}\text{Ca}$, $^{40}\text{Ca} + ^{48}\text{Ca}$, and $^{48}\text{Ca} + ^{48}\text{Ca}$. The reactions in which the superfluid nucleus ^{44}Ca is involved have rarely been investigated to date.

We use the harmonic oscillator basis in the xy plane and the Lagrange mesh in the z direction. The reaction axis (z axis) is described by spatial grid points (mesh) with the mesh parameter $\Delta z = 0.91$ fm with $N_z = 25$ grid points for the HFB initialization of the fragments.

A wide lattice space with $N_z = 50$ grid points is used for the dynamics of the two nuclei in head-on collision reactions. The quantum numbers of the harmonic oscillator eigenfunctions in the xy plane are restricted to $n_x + n_y \leq 5$. The harmonic oscillator parameters are $\hbar\omega_x = \hbar\omega_y = 11.6$ MeV. The distance between the initial center-of-mass coordinates of the two nuclei is 22.75 fm. The unit time step of dynamics is $\Delta t = 0.3$ fm/c, and we performed density-constrained calculations every 20 time steps.

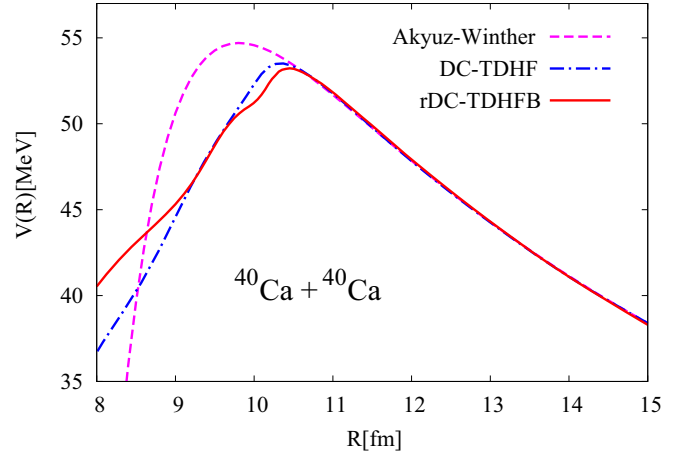


FIG. 1. Nucleus-nucleus interaction potential $V(R)$ for the $^{40}\text{Ca} + ^{40}\text{Ca}$ system obtained from rDC-TDHFB calculations using Eq. (8) at $E_{\text{c.m.}} = 55$ MeV (red solid line) compared with the result of the DC-TDHF method at $E_{\text{c.m.}} = 55$ MeV (blue dot-dashed line). The pink dashed line stands for the Akyuz-Winther phenomenological potential.

A. Nucleus-nucleus interaction potential

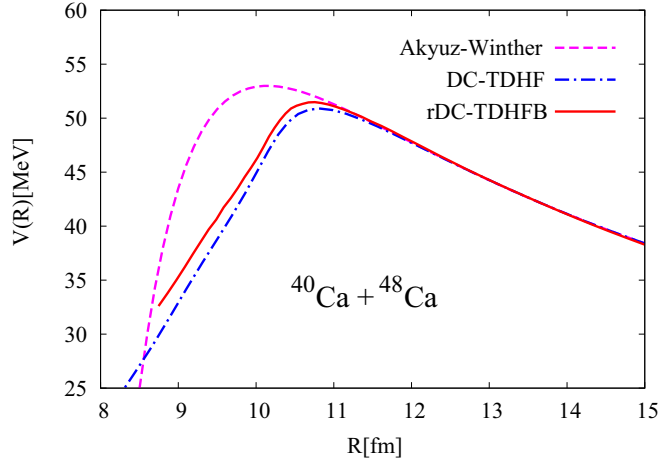
The nucleus-nucleus (N-N) interaction potential can be obtained as

$$V(R) = E_{\text{DC}}(R) - E_1 - E_2, \quad (8)$$

where $E_{\text{DC}}(R)$ is the total energy of the density-constrained state in Eq. (7) while E_1 and E_2 are the binding energies of the two colliding nuclei obtained from the static HFB calculations with the same GOGNY effective nucleon-nucleon interaction. R is the relative distance between the two centers of mass in the left and right regions of the fusing systems, obtained in the same way as in [34].

With the aid of the real-space density-constrained scheme of the rDC-TDHFB method proposed in Sec. II, we have calculated the N-N interaction potentials of the head-on collisions of $^{40}\text{Ca} + ^{40}\text{Ca}$, $^{40}\text{Ca} + ^{44}\text{Ca}$, and $^{40}\text{Ca} + ^{48}\text{Ca}$ systems at the initial energy $E_{\text{c.m.}} = 55$ MeV. The results are shown in Figs. 1–3, and are compared with the results obtained from the DC-TDHF method [35] and the Akyüz-Winther phenomenological model [36,37]. Here the TDHF trajectories are simulated by the SKY3D TDHF Code [38] with full Skyrme SV-bas parametrization. This code has been used to study the various fusion reaction systems.

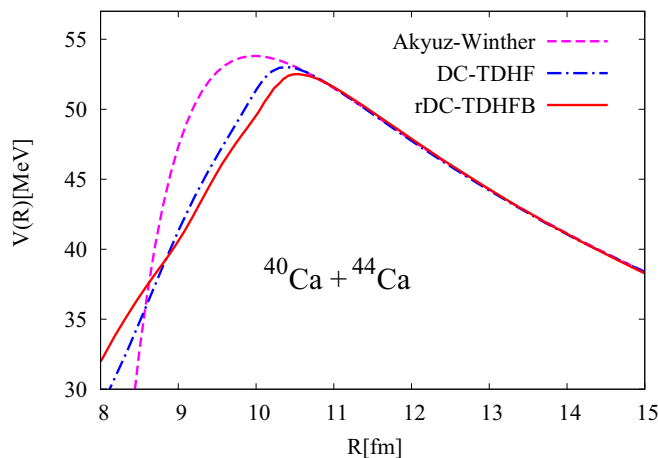
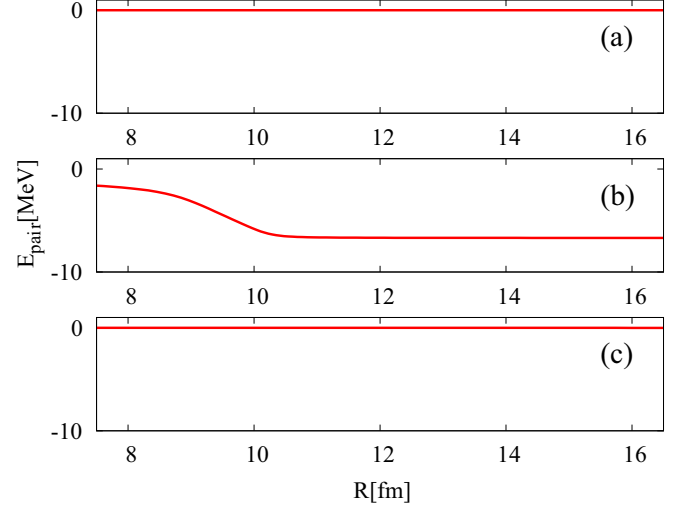
For the $^{40}\text{Ca} + ^{40}\text{Ca}$ system, Fig. 1 shows that the barrier height of the rDC-TDHFB potential $V(R)$ in Eq. (8) at the center-of-mass energy $E_{\text{c.m.}} = 55$ MeV is 53.23 MeV, with a corresponding R value of 10.44 fm. The barrier height calculated with DC-TDHF is 53.51 MeV at $R = 10.37$ fm. Both are significantly lower than the macroscopic Akyüz-Winther phenomenological potential. It is noteworthy that there is a general consensus that the effects of pairing play an important role for obtaining good initial states of projectile and target nuclei, as well as obtaining realistic density-constrained solutions when a single composite is formed. During a collision the effects of pairing are washed away due to the high

FIG. 2. The same as Fig. 1 but for $^{40}\text{Ca} + ^{48}\text{Ca}$.

excitations. In this sense, the pairing effects are minimal for the reaction $^{40}\text{Ca} + ^{40}\text{Ca}$ because of the double closed-shell structure of ^{40}Ca . This conclusion is consistent with the results obtained in [15] where the authors have claimed that the superfluidity does not bring an additional energy dependence of the potential.

As shown in Figs. 2 and 3, the asymmetrical $^{40}\text{Ca} + ^{48}\text{Ca}$ and $^{40}\text{Ca} + ^{44}\text{Ca}$ head-on collisions present relatively lower fusion barriers. The height of the potential barrier of $^{40}\text{Ca} + ^{44}\text{Ca}$ ($^{40}\text{Ca} + ^{48}\text{Ca}$) at the center-of-mass energy $E_{\text{c.m.}} = 55$ MeV is 52.51 MeV (51.48 MeV) at $R = 10.54$ fm (10.76 fm), respectively. The barrier heights calculated by DC-TDHF are 53.01 and 50.74 MeV at $R = 10.40$ and 10.82 fm. Here it should be mentioned that the effects of the pairing correlation should be important for obtaining the ground state of the superfluidity nucleus ^{44}Ca , but this point is not obviously shown in Fig. 3, because the property of ground state, described by the binding energies E_1 and/or E_2 , has been extracted from $E_{\text{DC}}(R)$ according to the definition of $V(R)$ in Eq. (8).

In general, there is a large uncertainty in predicting the form of the potential in macroscopic phenomenological ap-

FIG. 3. The same as Fig. 1 but for $^{40}\text{Ca} + ^{44}\text{Ca}$.FIG. 4. Pairing energy of the (a) $^{40}\text{Ca} + ^{40}\text{Ca}$ (b) $^{40}\text{Ca} + ^{44}\text{Ca}$ (c) $^{40}\text{Ca} + ^{48}\text{Ca}$ systems with the energy $E_{\text{c.m.}} = 55$ MeV are plotted with respect to collective coordinate R .

proaches when the two nuclei strongly overlap [39,40]. In the microscopic rDC-TDHF method, the dynamical changes of the pairing effects as well as density profiles are properly taken into account in Eq. (1). The pairing energy begins to change significantly around the barrier, and plays an important role in the fusion across the barrier of two nuclei to form a complex nucleus.

In order to clarify the effects of pairing, we calculate the pairing energy,

$$E_{\text{pair}} = \frac{1}{4} \sum_{\alpha\beta\gamma\delta} \bar{v}_{\alpha\beta\gamma\delta} \kappa_{\alpha\beta}^* \kappa_{\gamma\delta}, \quad (9)$$

where $\bar{v}_{\alpha\beta\gamma\delta}$ represents the Gaussian part of the two-body matrix elements, for $^{40}\text{Ca} + ^{40}\text{Ca}$, $^{40}\text{Ca} + ^{44}\text{Ca}$, and $^{40}\text{Ca} + ^{48}\text{Ca}$ systems at $E_{\text{c.m.}} = 55$ MeV. The results are shown in Fig. 4. It is clear that the pairing energy is very small in the reactions of $^{40}\text{Ca} + ^{40}\text{Ca}$ and $^{40}\text{Ca} + ^{48}\text{Ca}$. On the other hand, in the reaction $^{40}\text{Ca} + ^{44}\text{Ca}$, the pairing energy is kept nearly constant in the approach stage of the reaction, which can be attributed to the superfluidity of ^{44}Ca . After the two nuclei get together, there is an obvious change in the pairing energy and the pairing correlation becomes weaker and weaker. This change of the pairing effects is related to the excitation of the fused system, which could be accounted for in the constraints within the rDC-TDHF equation (1). The occurrence of internal excitation will reduce the pairing correlation in the fused system.

To conclude this subsection, let us show the convergence properties of rDC-TDHF. In order to assess the quality of convergence of Eq. (5), we define the quantities $\delta_{\rho}^{(n)}$ and $\delta_{\kappa}^{(n)}$ for the n th iteration as

$$\delta_{\rho}^{(n)} = \int d\mathbf{r} |\rho^{(n)}(\mathbf{r}) - \rho^{(0)}(\mathbf{r})|, \quad (10)$$

$$\delta_{\kappa}^{(n)} = \int d\mathbf{r} |\kappa_{\uparrow\downarrow}^{(n)}(\mathbf{r}) - \kappa_{\uparrow\downarrow}^{(0)}(\mathbf{r})|, \quad (11)$$

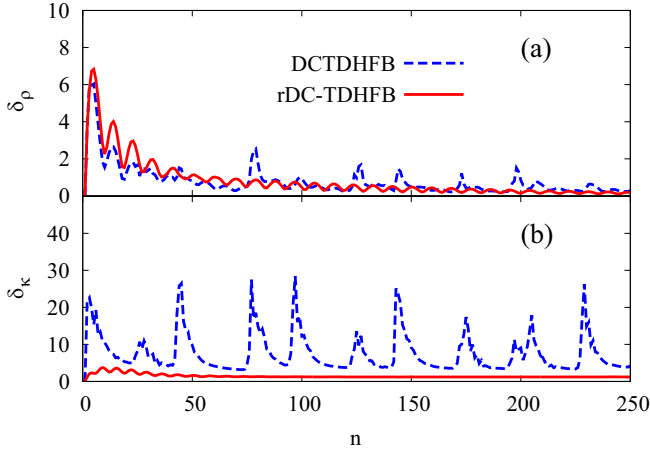


FIG. 5. The quality of iterative convergence of DCTDHFB (blue dashed line) and rDC-TDHFB (red solid line) methods for the $^{40}\text{Ca} + ^{44}\text{Ca}$ system at $R = 10.54$ fm.

where $\rho^{(0)}(\mathbf{r})$ and $\kappa_{\uparrow\downarrow}^{(0)}(\mathbf{r})$ are the instantaneous TDHFB particle and pairing densities, and $\rho^{(n)}(\mathbf{r})$ and $\kappa_{\uparrow\downarrow}^{(n)}(\mathbf{r})$ are the cases of the n th iteration. As the number of iterations n increases, when $\delta_{\rho}^{(n)}$ and $\delta_{\kappa}^{(n)}$ stably tend to a required small value simultaneously, the iteration will be stopped. In the DCTDHFB case [15], $\delta_{\kappa}^{(n)}$ is defined as

$$\delta_{\kappa}^{(n)} = \sum_{ij} ||\kappa_{ij}^{(n)}| - |\kappa_{ij}^{(0)}||, \quad (12)$$

where $\kappa_{ij}^{(0)}$ is the instantaneous TDHFB pairing tensor, and $\kappa_{ij}^{(n)}$ is the case of the n th iteration. As an example, Fig. 5 shows the quality of iterative convergence of the $^{40}\text{Ca} + ^{44}\text{Ca}$ fusion reaction at the barrier ($R = 10.54$ fm) calculated by rDC-TDHFB and DCTDHFB methods. For the rDC-TDHFB method, both $\delta_{\rho}^{(n)}$ and $\delta_{\kappa}^{(n)}$ smoothly and stably tend to their convergent values after several hundred iterations, much better than the case of the DCTDHFB method.

B. Collective kinetic energy

In principle, the solutions of both TDHF and TDHFB equations satisfy the equation of continuity if the two-body interactions are local [41,42]; i.e., the coordinate-space density $\rho(\mathbf{r}, t)$ should satisfy,

$$\frac{d\rho(\mathbf{r}, t)}{dt} = -\nabla \cdot \mathbf{j}(\mathbf{r}, t), \quad (13)$$

where $\mathbf{j}(\mathbf{r}, t)$ is the particle current. In TDHF theory, $\rho(\mathbf{r}, t)$ and $\mathbf{j}(\mathbf{r}, t)$ are defined by using single-particle states,

$$\rho(\mathbf{r}) = \sum_{\alpha} v_{\alpha}^2 \phi_{\alpha}(\mathbf{r}) \phi_{\alpha}^*(\mathbf{r}),$$

$$\mathbf{j}(\mathbf{r}) = \frac{1}{2i} \sum_{\alpha} v_{\alpha}^2 (\phi_{\alpha}^*(\mathbf{r}) \vec{\nabla} \phi_{\alpha}(\mathbf{r}) - \phi_{\alpha}(\mathbf{r}) \vec{\nabla} \phi_{\alpha}^*(\mathbf{r})),$$

where v_{α} equals 1 for occupied states or 0 for unoccupied states. This definition has been used in various realistic calculation, as in [34,35].

In the framework of the TDHFB theory, we begin with the TDHFB equations and get the equation of continuity in Eq. (13). Paying attention to the conservation property of the density and current, we adopt the expression of the particle current as

$$\mathbf{j}(\mathbf{r}) = \frac{1}{2i} \sum_{\alpha\beta} \rho_{\alpha\beta} [\phi_{\alpha}(\mathbf{r}) \vec{\nabla} \phi_{\beta}^*(\mathbf{r}) - \phi_{\beta}^*(\mathbf{r}) \vec{\nabla} \phi_{\alpha}(\mathbf{r})] \delta_{\sigma_{\alpha}\sigma_{\beta}}, \quad (14)$$

where the density matrix $\rho_{\alpha\beta}$ is the same as in Eq. (2a) constructed from V matrix in the TDHFB theory.

Note that this particle current, defined by matrix V , contains the effects of all the dynamical effects and the pairing correlations in the sense of the TDHFB theory. With the help of the particle current $\mathbf{j}(\mathbf{r})$ defined in Eq. (14), the collective kinetic energy of the system can be expressed in the same form as in the TDHF theory [34,35]:

$$E_{\text{kin}}^{\text{coll}} = \frac{\hbar^2}{2m} \int \frac{j^2(\mathbf{r})}{\rho(\mathbf{r})} d^3r. \quad (15)$$

The particle current $\mathbf{j}(\mathbf{r})$ is a key quantity to calculate the excitation energy in microscopic many-body theories, as discussed in the next subsection.

C. Effective mass parameter

In the dynamic calculation of TDHFB theory, the total energy of the system can be interpreted as the sum of static energy without collective motion, $E_{\text{DC}}(R)$, the collective kinetic energy $E_{\text{kin}}^{\text{coll}}(R)$, and the internal excitation energy $E^*(R)$. Therefore, the internal excitation energy can be obtained as

$$E^* = E_{\text{TDHFB}} - E_{\text{DC}}(R) - E_{\text{kin}}^{\text{coll}}, \quad (16)$$

Following the procedures of [35], one can easily obtain the effective mass parameter of the relative motion by energy conservation, as

$$M(R) = \frac{2[E_{\text{c.m.}} - V(R) - E^*(R)]}{\dot{R}^2}, \quad (17)$$

where the internal excitation energy is subtracted, because it is not part of the collective kinetic energy [35].

Figure 6 shows the effective mass parameters for the $^{40}\text{Ca} + ^{40}\text{Ca}$, $^{40}\text{Ca} + ^{44}\text{Ca}$, and $^{40}\text{Ca} + ^{48}\text{Ca}$ head-on collisions at $E_{\text{c.m.}} = 55$ MeV. The mass parameter describes the inertia of the total system against changes of its internal structure due to the relative motion of its fragments [43]. In many studies, the effective mass parameter is treated as the static reduced mass. However, due to density rearrangement and nucleon transfer, effective mass parameters have a very important effect on the fusion reaction by affecting the penetration probability. From the results of Fig. 6, the effective mass parameters obtained by rDC-TDHFB are similar to those obtained by DC-TDHF [35]. When the two nuclei of the fusion reaction are far apart, the effective mass parameters are the same as the reduced mass values. As the two nuclei approach closer to each other, the effective mass parameter increases and shows an obvious hump when the incident center-of-mass energy $E_{\text{c.m.}}$ approaches the barrier height [34,35].

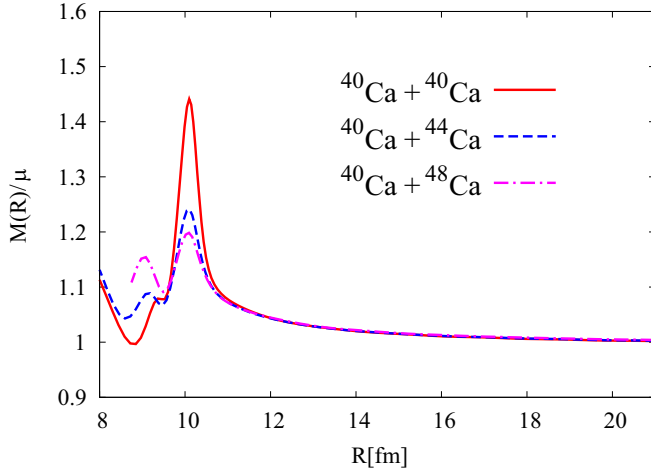


FIG. 6. Effective mass parameter $M(R)$ scaled by the constant reduced mass μ for head-on collisions of $^{40}\text{Ca} + ^{40,44,48}\text{Ca}$ at $E_{\text{c.m.}} = 55$ MeV.

D. Fusion cross section

Let us now calculate the fusion cross section, which is treated as the main objective of this paper. As stated in Sec. I, the fusion process with sub-barrier energies can be described as the barrier penetration of the full many-body system. In the quantum perspective, the fusion cross sections at a specific $E_{\text{c.m.}}$ can be obtained through

$$\sigma_{\text{fus}}(E_{\text{c.m.}}) = \frac{\pi \hbar^2}{2\mu E_{\text{c.m.}}} \sum_{l=0}^{\infty} (2l+1) T_l(E_{\text{c.m.}}), \quad (18)$$

where μ is the constant reduced mass that changes with different reactions, T_l is the barrier penetration probability of the l th angular momentum channel.

Following the great detailed procedures given in [35,44], the fusion barrier penetration probability $T_l(E_{\text{c.m.}})$ is obtained through numerical integration of the Schrödinger equation

$$\left[-\frac{\hbar^2}{2M(R)} \frac{d^2}{dR^2} + V(R) + \frac{l(l+1)\hbar^2}{2M(R)R^2} - E_{\text{c.m.}} \right] \psi_l = 0, \quad (19)$$

where ψ_l is the radial function for the l th partial wave, and the N-N potential $V(R)$ and effective mass parameter $M(R)$ are given in Eqs. (8) and (17), which included all of the dynamical features of TDHFB trajectory. Here the transfer matrix method [35,44] is adopted to calculate the penetration probabilities. By this method, we can accurately calculate the penetration probabilities across arbitrary potential barriers in both sub- and over-barrier regions.

Paying attention to the fact that the dependence of the potential barrier and the effective mass parameter on the excitation energy is moderate, the calculations were carried out at $E_{\text{c.m.}} = 55$ MeV, which is a little higher than the barrier.

Figures 7 and 8 show the fusion cross sections for the symmetrical $^{40}\text{Ca} + ^{40}\text{Ca}$ and asymmetrical $^{40}\text{Ca} + ^{48}\text{Ca}$ head-on collisions calculated using the N-N potentials of rDC-TDHFB and DC-TDHF methods in Figs. 1 and 2. It is clear that the results of both rDC-TDHFB and DC-TDHF methods finely reproduce the experimental data [24,25,27,28], much better

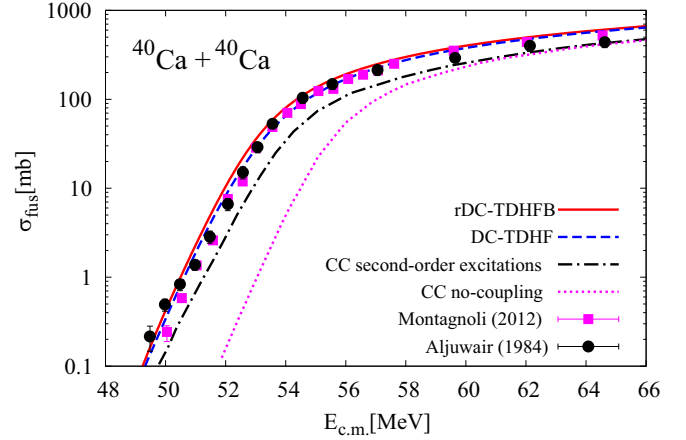


FIG. 7. Fusion cross sections for $^{40}\text{Ca} + ^{40}\text{Ca}$ obtained from the rDC-TDHFB potential and DC-TDHF potential at the same $E_{\text{c.m.}} = 55$ MeV. Results of the coupled channel calculations with no coupling (pink dotted line) and with second-order excitation (black dot-dashed line) are taken from Fig. 1 in Ref. [30]. The experimental data are taken from Aljuwair [24] and Montagnoli [28].

than the results of the coupled-channel approaches with the no coupling and/or with second-order excitation approximations in Ref. [30]. Note that our results with DC-TDHF by the SKY3D TDHF code [38] with full Skyme SV-bas parametrization are consistent with the ones reported in [34].

Here we would like to mention that, because of the theoretical limitation of TDHF theory, to date, the systematic investigation of the collision processes in which the superfluid nuclei are involved has been difficult from the standpoint of the microscopic quantum many-body theory. From Figs. 7 and 8, we gained confidence that our new scheme of the rDC-TDHFB method in Eq. (1) could be a reliable and useful starting point to study the collision of normal and superfluid nuclei.

Now, let us apply our proposed rDC-TDHFB method to the case of the reaction $^{40}\text{Ca} + ^{44}\text{Ca}$, where ^{44}Ca is a superfluid nucleus on the neutron side and the pairing energy of the

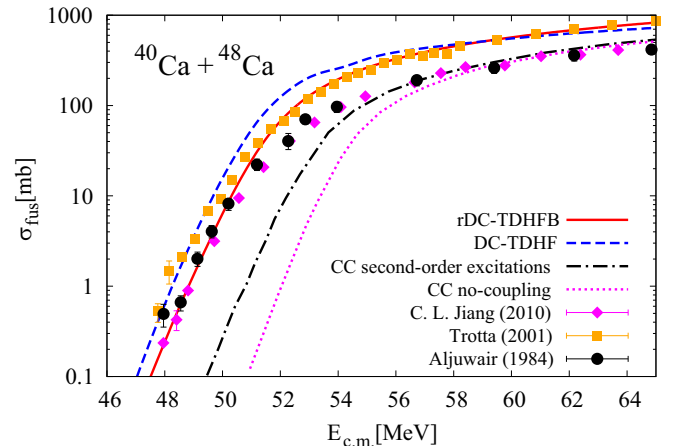


FIG. 8. The same as Fig. 7 but for $^{40}\text{Ca} + ^{48}\text{Ca}$. The experimental data are taken from Aljuwair [24], Trotta [25], and Jiang [27].

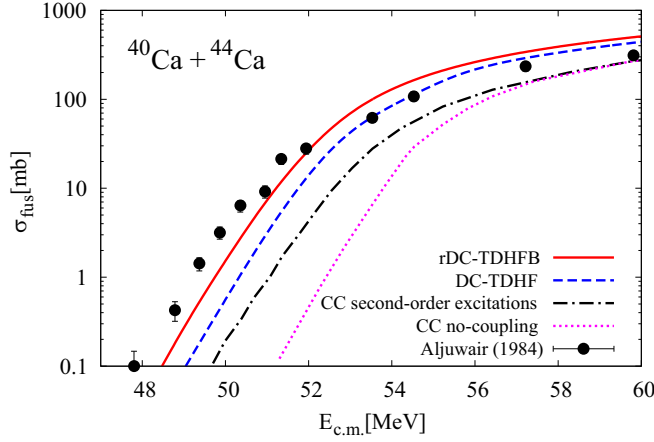


FIG. 9. The same as in Fig. 7 but for $^{40}\text{Ca} + ^{44}\text{Ca}$. The experimental data are taken from Aljuwair [24].

entrance channel is $E_{\text{pair}} = -6.69$ MeV. The results of the fusion cross section are presented in Fig. 9. It is remarkable that the cross sections calculated by our rDC-TDHFB scheme are much larger than those of DC-TDHF, thus rDC-TDHFB greatly enhances the fusion probability, especially in the sub-barrier energy region. The rDC-TDHFB results rather satisfactorily reproduce the experimental data, and again the rDC-TDHFB results are better than the coupled-channel approaches in near- and sub-barrier energy regions.

Finally, we consider the collisions between the two super-fluid nuclei, where the pairing correlations are fully active. Figure 10 shows the fusion potential of $^{44}\text{Ca} + ^{44}\text{Ca}$ reactions at $E_{\text{c.m.}} = 53$ MeV, and compares with the results of zero gauge angle in [15]. It seems that the N-N potential with rDC-TDHFB is lower than the results taken from [15]. Because the main GOGNY-TDHFB code and the parameters used in this paper are the same as in [15], as discussed in Sec. II, the possible reason for this difference may be that the rDC-TDHFB method proposed in this paper can squeeze

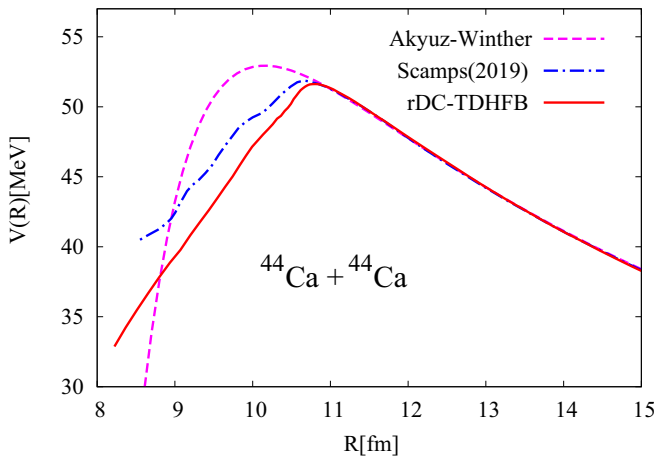


FIG. 10. The same as Fig. 1 but for $^{44}\text{Ca} + ^{44}\text{Ca}$ fusion reactions at $E_{\text{c.m.}} = 53$ MeV. The data of Scamp's method are taken from the results with zero gauge angle of [15].

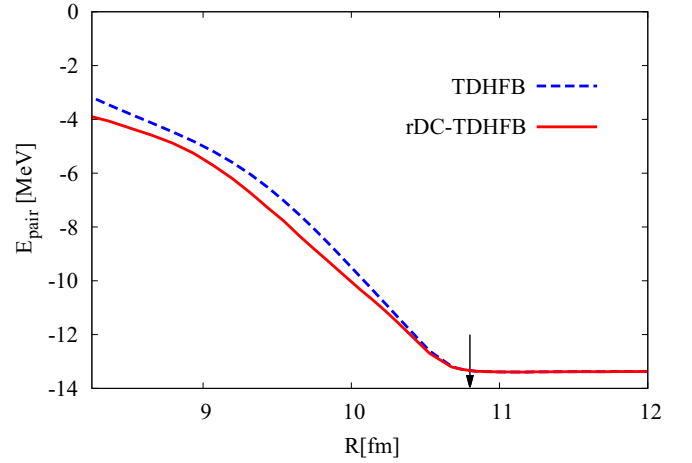


FIG. 11. Pairing energy of the $^{44}\text{Ca} + ^{44}\text{Ca}$ system by rDC-TDHFB method at $E_{\text{c.m.}} = 53$ MeV is plotted with respect to collective coordinate R , and compared with the pairing energy of TDHFB trajectory. The black arrow on the x axis indicates the barrier position corresponding to the fusion reaction.

out the collective kinetic and/or excitation energies from the total energy of TDHFB trajectory more efficiently. The DCTDHF method constrains the norm of all the matrix elements κ_{ij} , which are intrinsic variables, thus the pairing energy is conserved after the density-constrained calculation (Fig. 8 of Ref. [15]). In this paper, the rDC-TDHFB method constrains the pairing densities $\kappa_{\uparrow\downarrow}(\mathbf{r})$, which are collective variables. In this scheme, the pairing energy is different between TDHFB and rDC-TDHFB. We show the comparison of pairing energy from rDC-TDHFB and TDHFB calculations in Fig. 11, for the $^{44}\text{Ca} + ^{44}\text{Ca}$ system. The difference of pairing energy between TDHFB and rDC-TDHFB is consistent with the result shown in Fig. 10.

The potential in Fig. 10 has been used to calculate the fusion cross section of $^{44}\text{Ca} + ^{44}\text{Ca}$, as shown in Fig. 12. To highlight the differences among all four systems, we also plot the theoretical fusion cross sections of $^{40}\text{Ca} + ^{40}\text{Ca}$, $^{40}\text{Ca} + ^{44}\text{Ca}$, and $^{40}\text{Ca} + ^{48}\text{Ca}$. The

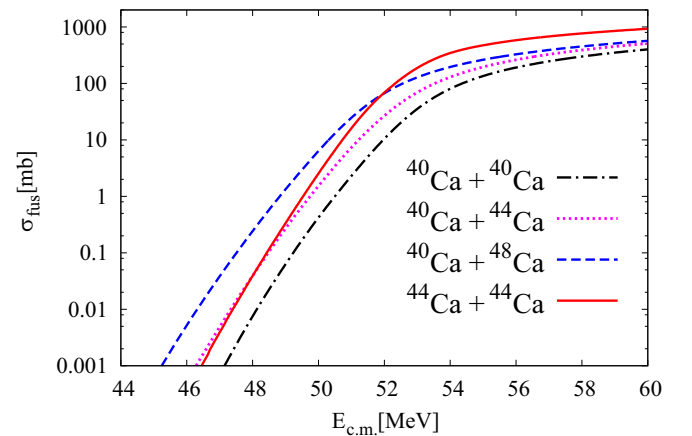


FIG. 12. Fusion cross sections obtained from the rDC-TDHFB approach.

TABLE I. Ground state Q values (in MeV) for two-neutron transferring channels.

System	Q_{2n}
$^{40}\text{Ca} + ^{40}\text{Ca}$	-9.13
$^{40}\text{Ca} + ^{44}\text{Ca}$	0.77
$^{40}\text{Ca} + ^{48}\text{Ca}$	2.61
$^{44}\text{Ca} + ^{44}\text{Ca}$	-1.25

cross sections for $^{40}\text{Ca} + ^{40}\text{Ca}$, $^{40}\text{Ca} + ^{44}\text{Ca}$, and $^{40}\text{Ca} + ^{48}\text{Ca}$ are typical. For the reaction $^{40}\text{Ca} + ^{40}\text{Ca}$, the cross section falls much faster with decreasing energy and becomes approximately an order of magnitude smaller than those for $^{40}\text{Ca} + ^{44}\text{Ca}$ and $^{40}\text{Ca} + ^{48}\text{Ca}$. With the increasing neutron richness, the fusion cross section from $^{40}\text{Ca} + ^{40}\text{Ca}$ through $^{40}\text{Ca} + ^{44}\text{Ca}$ to $^{40}\text{Ca} + ^{48}\text{Ca}$ increases in the whole energy region. Consider the ground state Q values for two-neutron transfer channels of every system as given in Table. I; this can be attributed to the strong coupling to the two-neutron transfer channels with positive Q values [24,29,30].

Another interesting feature in Fig. 12 is that the fusion cross sections of $^{40}\text{Ca} + ^{48}\text{Ca}$ and $^{44}\text{Ca} + ^{44}\text{Ca}$, which correspond to the same composite systems, intersect one another around the barrier energy. The cross sections of $^{44}\text{Ca} + ^{44}\text{Ca}$ are larger than the one of $^{40}\text{Ca} + ^{48}\text{Ca}$ when the energy $E_{\text{c.m.}}$ is above the barrier, while they are smaller when the energy $E_{\text{c.m.}}$ is below the barrier. One possible mechanism of this result could also be the effect of particle transfer. However, because the superfluid nuclei ^{44}Ca is softer with respect to the collective modes than the two doubly magic nuclei ^{40}Ca and ^{48}Ca , the influence of the excitations of collective motions and some other excitations of collective modes should be studied further. We leave this subject to our further investigation.

IV. SUMMARY

The theoretical understanding of sub-barrier heavy ion fusion reactions remains a significant challenge even to this day. Time-dependent density functional theory provides a self-consistent and elaborate microscopic framework to study the heavy-ion reactions.

In this paper, we proposed a real-space particle- and pairing-density-constrained scheme of the microscopic TD-HFB theory. The proposed rDC-TDHFB scheme was applied to analyze the reactions of nuclei with and without pairing correlations, such as $^{40}\text{Ca} + ^{40}\text{Ca}$, $^{40}\text{Ca} + ^{44}\text{Ca}$, $^{40}\text{Ca} + ^{48}\text{Ca}$, and $^{44}\text{Ca} + ^{44}\text{Ca}$. The results satisfactorily reproduce the experimental data of the sub-barrier cross sections, illustrating the feasibility of the rDC-TDHFB scheme.

Because the constrained densities in the rDC-TDHFB scheme are the corresponding instantaneous TDHFB densities at every specific time, both the nucleus-nucleus interaction potential and the mass parameter in collective space include the dynamical effects and various excitations described by the particle and pairing densities. Therefore this method could provide a reliable description of nuclear reactions where the pairing effects play one of the central roles in the nuclear properties.

In near future, it will be very interesting to use this scheme to investigate the dynamical roles of the pairing correlations in the reactions of exotic nuclei, as well as in the fission process of heavy nuclei.

ACKNOWLEDGMENTS

We are deeply indebted to Yukio Hashimoto for his valuable discussions. This work was partly supported by the National Natural Science Foundation of China under Grants No. 11675018, No. 11735005, and No. 11790325. The numerical simulation was supported by the HSCC of Beijing Normal University.

-
- [1] D. L. Hill and J. A. Wheeler, *Phys. Rev.* **89**, 1102 (1953).
 - [2] W. Nörenberg, *Phys. Lett. B* **104**, 107 (1981).
 - [3] K. Washiyama, D. Lacroix, and S. Ayik, *Phys. Rev. C* **79**, 024609 (2009).
 - [4] X. Jiang, S. Yan, and J. A. Maruhn, *Phys. Rev. C* **88**, 044611 (2013).
 - [5] J. Błocki and H. Flocard, *Nucl. Phys. A* **273**, 45 (1976).
 - [6] F. Barranco, G. Bertsch, R. Broglia, and E. Vigezzi, *Nucl. Phys. A* **512**, 253 (1990).
 - [7] G. Bertsch, *Nucl. Phys. A* **574**, 169 (1994).
 - [8] G. F. Bertsch and A. Bulgac, *Phys. Rev. Lett.* **79**, 3539 (1997).
 - [9] S. Ebata, T. Nakatsukasa, T. Inakura, K. Yoshida, Y. Hashimoto, and K. Yabana, *Phys. Rev. C* **82**, 034306 (2010).
 - [10] T. K. Steinbach, J. Vadas, J. Schmidt, C. Haycraft, S. Hudan, R. T. deSouza, L. T. Baby, S. A. Kuvin, I. Wiedenhöver, A. S. Umar, and V. E. Oberacker, *Phys. Rev. C* **90**, 041603(R) (2014).
 - [11] G. Scamps, D. Lacroix, G. F. Bertsch, and K. Washiyama, *Phys. Rev. C* **85**, 034328 (2012).
 - [12] B. Avez, C. Simenel, and P. Chomaz, *Phys. Rev. C* **78**, 044318 (2008).
 - [13] I. Stetcu, A. Bulgac, P. Magierski, and K. J. Roche, *Phys. Rev. C* **84**, 051309(R) (2011).
 - [14] Y. Hashimoto, *Phys. Rev. C* **88**, 034307 (2013).
 - [15] G. Scamps and Y. Hashimoto, *Phys. Rev. C* **100**, 024623 (2019).
 - [16] A. S. Umar and V. E. Oberacker, *Phys. Rev. C* **74**, 021601(R) (2006).
 - [17] A. S. Umar and V. E. Oberacker, *Phys. Rev. C* **77**, 064605 (2008).
 - [18] D. Baye, *Phys. Rep.* **565**, 1 (2015), the Lagrange-mesh method.
 - [19] E. Perlińska, S. G. Rohoziński, J. Dobaczewski, and W. Nazarewicz, *Phys. Rev. C* **69**, 014316 (2004).
 - [20] D. D. Johnson, *Phys. Rev. B* **38**, 12807 (1988).
 - [21] A. Baran, A. Bulgac, M. M. Forbes, G. Hagen, W. Nazarewicz, N. Schunck, and M. V. Stoitsov, *Phys. Rev. C* **78**, 014318 (2008).
 - [22] P. Magierski, K. Sekizawa, and G. Wlazłowski, *Phys. Rev. Lett.* **119**, 042501 (2017).
 - [23] G. Scamps and D. Lacroix, *Phys. Rev. C* **87**, 014605 (2013).

- [24] H. A. Aljuwair, R. J. Ledoux, M. Beckerman, S. B. Gazes, J. Wiggins, E. R. Cosman, R. R. Betts, S. Saini, and O. Hansen, *Phys. Rev. C* **30**, 1223 (1984).
- [25] M. Trotta, A. M. Stefanini, L. Corradi, A. Gadea, F. Scarlassara, S. Beghini, and G. Montagnoli, *Phys. Rev. C* **65**, 011601(R) (2001).
- [26] A. Stefanini, G. Montagnoli, R. Silvestri, L. Corradi, S. Courtin, E. Fioretto, B. Guiot, F. Haas, D. Lebhertz, P. Mason, F. Scarlassara, and S. Szilner, *Phys. Lett. B* **679**, 95 (2009).
- [27] C. L. Jiang, A. M. Stefanini, H. Esbensen, K. E. Rehm, L. Corradi, E. Fioretto, P. Mason, G. Montagnoli, F. Scarlassara, R. Silvestri, P. P. Singh, S. Szilner, X. D. Tang, and C. A. Ur, *Phys. Rev. C* **82**, 041601(R) (2010).
- [28] G. Montagnoli, A. M. Stefanini, C. L. Jiang, H. Esbensen, L. Corradi, S. Courtin, E. Fioretto, A. Goasduff, F. Haas, A. F. Kifle, C. Michelagnoli, D. Montanari, T. Mijatović, K. E. Rehm, R. Silvestri, P. P. Singh, F. Scarlassara, S. Szilner, X. D. Tang, and C. A. Ur, *Phys. Rev. C* **85**, 024607 (2012).
- [29] S. Landowne, C. H. Dasso, R. A. Broglia, and G. Pollaro, *Phys. Rev. C* **31**, 1047 (1985).
- [30] H. Esbensen, S. H. Fricke, and S. Landowne, *Phys. Rev. C* **40**, 2046 (1989).
- [31] J. Gao, H. Zhang, X. Bao, J. Li, and H. Zhang, *Nucl. Phys. A* **929**, 9 (2014).
- [32] H. Esbensen, C. L. Jiang, and A. M. Stefanini, *Phys. Rev. C* **82**, 054621 (2010).
- [33] N. Rowley and K. Hagino, in The 10th International Conference on Nucleus-Nucleus Collisions (NN2009) [*Nucl. Phys. A* **834**, 110c (2010)].
- [34] R. Kesper, A. S. Umar, and V. E. Oberacker, *Phys. Rev. C* **85**, 044606 (2012).
- [35] X. Jiang, J. A. Maruhn, and S. Yan, *Phys. Rev. C* **90**, 064618 (2014).
- [36] O. Akyüz and A. Winther, in *Proceedings of the Enrico Fermi International School of Physics, 1979*, edited by R. A. Broglia (North-Holland, Amsterdam, 1979).
- [37] C. K. Phookan and K. Kalita, *Indian J. Phys.* **90**, 99 (2016).
- [38] J. Maruhn, P.-G. Reinhard, P. Stevenson, and A. Umar, *Comput. Phys. Commun.* **185**, 2195 (2014).
- [39] C. H. Dasso and G. Pollaro, *Phys. Rev. C* **68**, 054604 (2003).
- [40] S. Mişicu and H. Esbensen, *Phys. Rev. Lett.* **96**, 112701 (2006).
- [41] J.-P. Blaizot and G. Ripka, *Quantum Theory of Finite Systems* (MIT Press, Cambridge, MA, 1985).
- [42] P. Ring and P. Schuck, *The Nuclear Many-Body Problem* (Springer-Verlag, New York, 1980).
- [43] K. Goeke, F. Grümmer, and P.-G. Reinhard, *Ann. Phys. (NY)* **150**, 504 (1983).
- [44] Y. Ando and T. Itoh, *J. Appl. Phys.* **61**, 1497 (1987).